Metasurface-Based Tapered Waveguide Slot Array Antennas for Wide Angular Scanning in a Narrow Frequency Band

Aofang Zhang, Rui Yang, Dong Li, Bowei Hu, Zhenya Lei, and Yongchang Jiao

***Abstract*— We demonstrate the frequency scanning performances from a linearly tapered rectangular waveguide slot array antenna using the spatial angular filtering metasurface. To be more specific, the metasurface at the narrow side of the waveguide is shown to be capable of releasing different wavelength energies when under the illuminations from different incident angles, while the tapered waveguide is proposed to mimic the oblique incidence and thus functions as the excitation of the antenna. Such frequency scanning radiations can also be extended for both orthogonally polarized electromagnetic fields when integrated with another polarization selective surface properly behind the metasurface. Finally, we carry out the experiments to verify our proposed designs and demonstrate the excellent beam-scanning performances when the frequency is changing.**

***Index Terms*— Frequency scanning, metasurfaces, waveguide slot array antennas.**

I. Introduction

WAVEGUIDE slot array antennas, possessing the merits of low profile, lightweight, and high aperture efficiency, are widely used in the communication systems. Especially, the emitting phase through the slots of such antennas is varied with frequencies, leading to the scanned beams as the frequency changes [1]–[10]. So far, different types of waveguides have been employed in the frequency scanning designs, such as rectangular waveguide [1]–[3], ridge gap waveguide [4], parallel plate waveguide [5], and substrate integrated waveguide [6]–[10], demonstrating the frequency-dependent leakages with steerable beams. Among all these investigations, the redirected radiation is basically determined by the phase difference between adjacent radiating slots, which thus fundamentally relies on the variation of the waveguide wavelength λ_g. As a result, such antennas normally radiate in the direction of $\arcsin(\lambda_0/\lambda_g - \lambda_0/2p)$ with the preset separations p between the adjacent slots [11]. In this way, it generally requires a wide bandwidth for the beam scanning performances due to the fact that λ_g varies slowly with the frequency. For example, the maximum scanning angle range is 28.8° in the WR62 waveguide over the entire operating frequency range from 12.4 to 18.0 GHz with 36.8% fractional bandwidth (FBW) when p is equal to the half waveguide wavelength at 15 GHz. Such a case may become unacceptable especially in the contemporary communications with limited spectrum resources, and it is always desired to achieve a wider angular scanning radiation within a small frequency band.

The metasurfaces have been enormously studied and rapidly adopted in wide research areas due to its powerful abilities to control electromagnetic (EM) fields, where gradient-index metasurfaces devised from the generalized Snell's laws [12] are proved to be an effective way to realize frequency scanning radiations [13]–[16]. Especially, programmable and coding metasurfaces have been proposed and demonstrated to be capable of realizing beam-scanning performances at a single frequency through electrically tuning the loaded diodes [17]–[20]. On the other hand, metasurfaces owning the functionality of spatial angular filtering (SAF) of the incident waves have also been observed and proposed as the qualified candidate for the frequency scanning designs [21]–[24], and above all the metasurface composed of periodic interconnected complementary split ring resonators [23], [24], has demonstrated that the transmission frequencies of incident plane waves can be tuned 3% FBW by changing the incident angles from 0° to 30°. If we can apply such a kind of metasurface with SAF characteristics to waveguide slot array antennas, it may realize a wide scanning angle radiation within a small frequency range.

Based on these considerations, we propose an SAF metasurface-based tapered waveguide slot array antenna (TWSAA) design for the frequency scanning performances. More specifically, the metasurface at the narrow side of the waveguide is shown to be capable of releasing different wavelength energies when under the illuminations from different incident angles, while the tapered waveguide is proposed to mimic the oblique incidence and thus functions as the excitation of the antenna. We will also demonstrate that such a design can readily be extended to both orthogonally polarized EM fields by adding another polarization selective surface properly behind the metasurface. This paper is organized as follows. In Section II, the SAF metasurface is proposed

Manuscript received October 4, 2017; revised April 6, 2018; accepted May 9, 2018. Date of publication May 23, 2018; date of current version August 2, 2018. This work was supported in part by the National Natural Science Foundation of China under Grant 61671344 and Grant 61301072 and in part by the Fundamental Research Funds for the Central Universities from China under Grant JB160206 and Grant JBG160216. *(Corresponding author: Rui Yang.)*

The authors are with the School of Electronic Engineering, Xidian University, Xi'an 710071, China (e-mail: ruiyang.xidian@gmail.com).

Color versions of one or more of the figures in this paper are available online at http://ieeexplore.ieee.org.

Digital Object Identifier 10.1109/TAP.2018.2839902

and the transmission characteristics of the metasurface are demonstrated with the excitation of TE-polarized plane waves. In Section III, the linearly tapered rectangular waveguide is introduced and demonstrated to produce the equivalent TE-polarized plane waves with gradient varied oblique incidence. In Sections IV and V, the proposed metasurface-based TWSAAs are presented with both numerical simulations and experimental verifications. Finally, conclusions are drawn in Section VI.

II. Leakage From the Spatial Angular Filtering Metasurface

Let us start with the SAF metasurface consisting of periodic symmetrical oblique C-slits, as shown in Fig. 1(a). The oblique C-slits are etched on the metallic surface of the dielectric substrate, where the oblique C-slits are symmetrical in the y-direction. According to the image theory, the unit cell of the SAF metasurface could be equivalent to a single oblique C-slit sandwiched in the top and bottom PEC plates as shown in Fig. 1(b) when under the illuminations of the TE$_y$-polarized EM waves, where the additional PEC boundaries would equate the symmetrical structure when the E-field vector is in the y-direction. The incident TE$_y$-polarized EM waves can be expressed as

$$\begin{cases} \vec{E}_i = E_0 \hat{y} e^{-jk(x\sin\theta + z\cos\theta)} \\ \vec{H}_i = \dfrac{E_0}{\eta}(-\hat{x}\cos\theta + \hat{z}\sin\theta) e^{-jk(x\sin\theta + z\cos\theta)} \end{cases} \tag{1}$$

where θ is the incident angle, k is the wavenumber and $\eta = \sqrt{\mu_0/\varepsilon_0}$ is the wave impedance in free space. We can observe in Fig. 1(c) that the transmitted EM waves would be filtered into different monochromatic EM waves with different transmission angles by the metasurface under the illuminations of the TE$_y$-polarized composite plane EM waves. The first-order resonant frequency f_r of the C-slit can be estimated by the C-slit perimeter $D = d_1 + 2d_2 \approx c/(f_r\sqrt{2(\varepsilon_r+1)})$ [21], where c is the light velocity. We know that the EM waves will penetrate the periodic C-slits with greatly enhanced transmissions at the resonant frequency but the strong coupling between the symmetrical oblique C-slits in our case makes the resonant frequency f_r shift [23], [25], and vary with the incident angles, producing the SAF transmissions of the metasurface. For the demonstration, the transmission frequencies of our design can be tuned from 16.08 to 15.42 GHz when the incident angle is swept from 0° to 45°. One method to control the coupling intensity is to adjust the ratio d_1/D of the C-slit side length to the perimeter. Fig. 1(d) and (e) demonstrates the transmission properties of the metasurface when the C-slits having different side lengths d_1 and fixed perimeter D while the other parameters are the same as shown in Fig. 1(c). As shown in Fig. 1(d), we can observe that the resonant frequency is slightly increased when the incident angle remains the same and d_1/D increases, and this is due to the increased coupling with compact symmetrical C-slits. We can also observe in Fig. 1(e) that the Δf is getting larger as the adjacent symmetrical C-slits become closer, ranging from 0.38 to 1.04 GHz when d_1/D increases from 0.4 to 1.0.

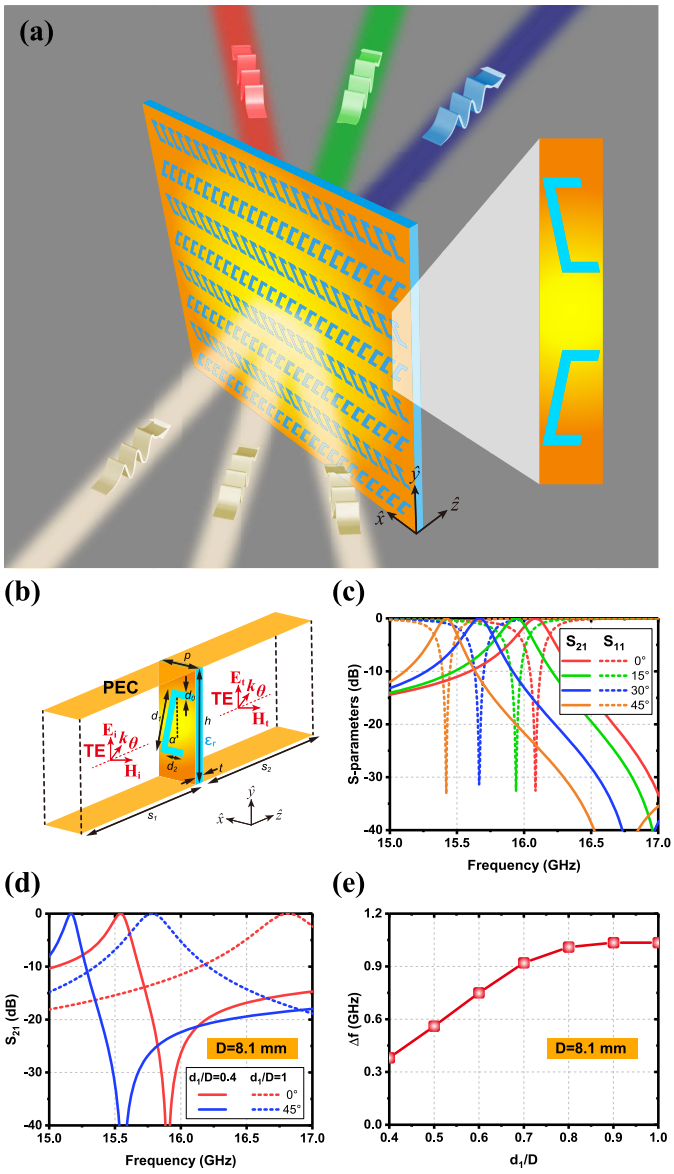

Fig. 1. SAF metasurface and its transmission characteristics. (a) SAF metasurface under the illuminations of TE$_y$-polarized EM fields, where white light beams represent the composite EM waves and red, green, and blue light beams represent the monochromatic EM waves from low to high frequencies, respectively. (b) Equivalent unit cell of the metasurface, where the PEC boundaries are equivalent to a symmetrical oblique C-slit in the y-direction. (c) Transmission and reflection coefficients for the metasurface with oblique incidence of TE$_y$-polarized EM fields, where the structural parameters are $d_0 = 0.3$ mm, $d_1 = 4.5$ mm, $d_2 = 1.8$ mm, $\alpha = 15°$, $p = 3$ mm, $h = 7.9$ mm, $t = 0.5$ mm, $s_1 = s_2 = 20$ mm, and $\varepsilon_r = 2.65$. (d) Transmission coefficients with $d_1/D = 0.4$ and $d_1/D = 1$ at different incident angles when $D = 8.1$ mm. (e) Transmission frequency tuning range from 0° to 45° incidence varied with d_1/D when $D = 8.1$ mm. In (d) and (e), the C-slit would be 7.82 mm in the y-direction when $d_1 = D = 8.1$ mm, and it should still be in the scope of the structure with 7.9 mm height.

III. Tapered Rectangular Waveguide for Gradient Varied Oblique Incidence

Now we consider applying the SAF metasurface to antenna realms for the frequency scanning performance, and the key issue of such an application is to generate the TE-polarized EM fields with gradient varied incident angles. We know

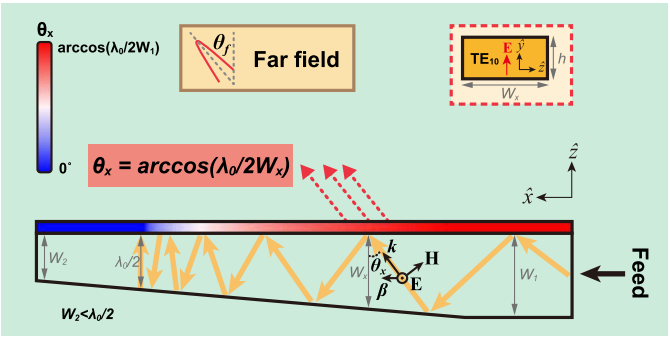

Fig. 2. Schematic of the propagation properties for the dominant mode TE_{10} in a tapered rectangular waveguide, where the TE_{10} mode is equivalent to the superposition of the zigzag propagating TE_y-polarized plane waves with gradient varied oblique incidence.

that the dominant mode TE_{10} in a rectangular waveguide is equivalent to the superposition of the zigzag propagating TE-polarized plane waves, and such characteristics of the EM field enable us to employ a tapered rectangular waveguide to mimic the TE-polarized plane waves for the gradient varied oblique incidence, as shown in Fig. 2, where the incident angles are different at different positions in the waveguide. The electric and magnetic fields of the TE_{10} mode in the tapered rectangular waveguide can be expressed as

$$\begin{cases} \vec{E} = -\hat{y}\, j2E_0 \sin\left(\dfrac{\pi z}{W_x}\right) e^{-j\beta x} \\ \vec{H} = \hat{x}\dfrac{2E_0}{\eta}\left(\dfrac{\lambda_0}{2W_x}\right)\cos\left(\dfrac{\pi z}{W_x}\right) e^{-j\beta x} \\ \qquad -\hat{z}\dfrac{j2E_0}{\eta}\sqrt{1-\left(\dfrac{\lambda_0}{2W_x}\right)^2}\sin\left(\dfrac{\pi z}{W_x}\right) e^{-j\beta x} \end{cases} \tag{2}$$

where W_x is the length of the rectangular waveguide wide side, $\beta = \sqrt{k^2 - (\pi/W_x)^2}$ is the propagation constant, and λ_0 is the wavelength in free space. If we define $\beta = k\sin\theta_x$, (2) can also be written as

$$\begin{cases} \vec{E} = E_0\hat{y}[e^{-jk(x\sin\theta_x + z\cos\theta_x)} - e^{-jk(x\sin\theta_x - z\cos\theta_x)}] \\ \vec{H} = \dfrac{E_0}{\eta}[(-\hat{x}\cos\theta_x + \hat{z}\sin\theta_x)e^{-jk(x\sin\theta_x + z\cos\theta_x)} \\ \qquad + (-\hat{x}\cos\theta_x - \hat{z}\sin\theta_x)e^{-jk(x\sin\theta_x - z\cos\theta_x)}]. \end{cases} \tag{3}$$

Comparing (3) with (1), we can clearly find the equivalent TE_y-polarized plane waves zigzag propagating with gradient varied oblique incidence and the incident angle would be

$$\theta_x = \arccos\left(\frac{\lambda_0}{2W_x}\right). \tag{4}$$

It is noted that the propagating wave will move forward slower when the incident angle θ_x become smaller. And when $W_x = \lambda_0/2$, the wave would stop to travel forward due to $\theta_x = 0°$ that corresponds to the cutoff condition of TE_{10} mode. Therefore, we should have W_2 less than $\lambda_0/2$ and the coverage of θ_x is, thus,

$$0 \le \theta_x \le \arccos\left(\frac{\lambda_0}{2W_1}\right). \tag{5}$$

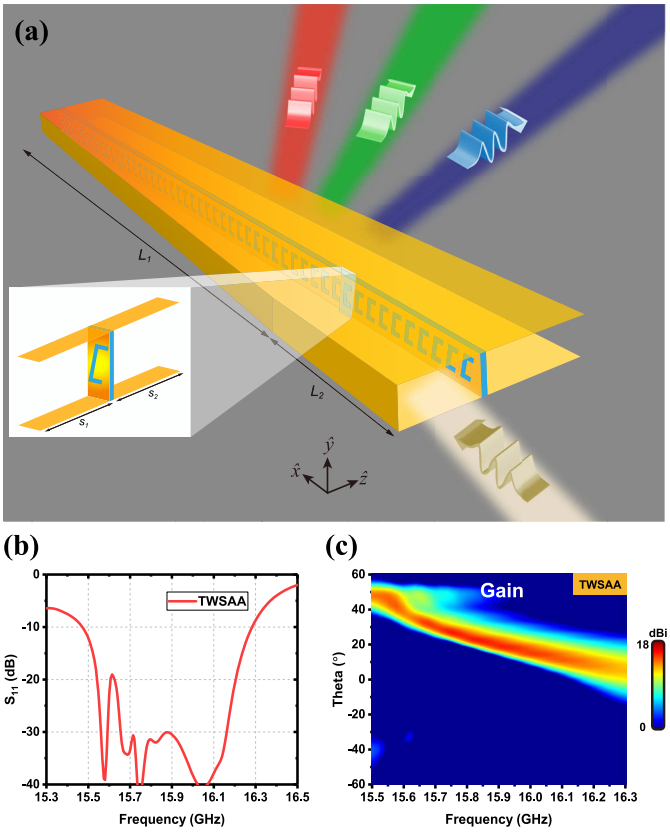

Fig. 3. Illustration of the TWSAA using the SAF metasurface. (a) Demonstration of the TWSAA, where white light beams represent the composite EM waves and red, green, and blue light beams represent the monochromatic EM waves from low to high frequencies, respectively. (b) Reflection coefficients of the TWSAA. (c) Far-field radiation performances of the TWSAA in xz-plane. In (b) and (c), the antenna parameters are $W_1 = 15.8$ mm, $W_2 = 7.9$ mm, $L_1 = 300$ mm, $L_2 = 30$ mm, $s_2 = 20$ mm, which is fed by WR62 waveguide, and other metasurface parameters are the same as shown in Fig. 1(c).

IV. Metasurface-Based Tapered Waveguide Slot Array Antennas

We now apply the SAF metasurface to the narrow side of the tapered waveguide to form the TWSAA, as shown in Fig. 3(a). Such a structure can be considered as the combination of periodic unit cells of Fig. 1(b) and an oblique metal face, where the long transitional parallel PEC boundaries are required to equate the symmetrical C-slits. Fig. 3(b) demonstrates the operating bandwidth of the TWSAA, and the reflection coefficient is less than -10 dB with good impedance matching over the frequency range approximately from 15.5 to 16.3 GHz. In the meanwhile, we can also observe in Fig. 3(c) that the main lobe in xz-plane can be scanned from 47° to 5° through tuning the frequency from 15.5 to 16.3 GHz with 5% FBW.

Each C-slit of the metasurface can be considered as a radiator and the far-field phase difference emitted by the adjacent unit cells is $\beta p - kp\sin\theta_f$, where θ_f is the radiating direction. The far-fields can thus be estimated as

$$F \approx \sum_n F_n e^{jn(\beta p - kp\sin\theta_f)} \tag{6}$$

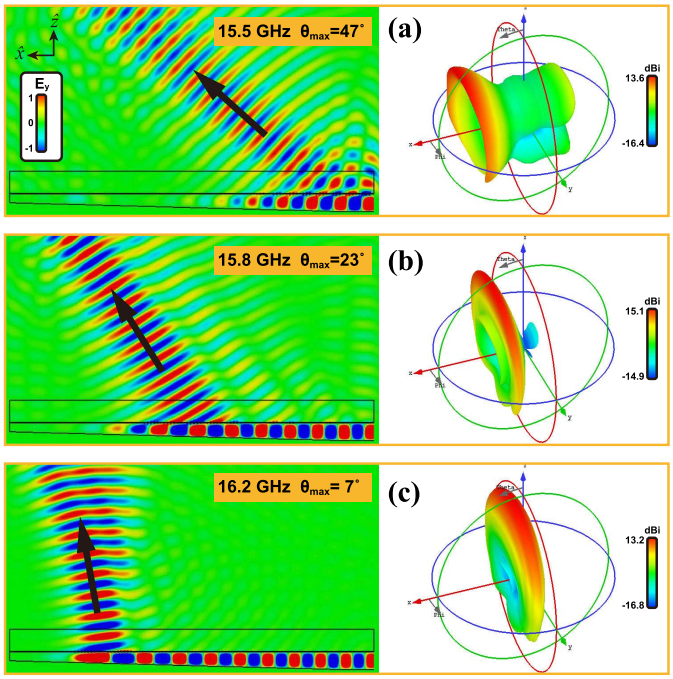

Fig. 4. Near-field distributions with E_y component and 3-D far-field radiation patterns of the TWSAA at different frequencies, where the E-fields are normalized by 800 V/m. (a) 15.5, (b) 15.8, and (c) 16.2 GHz.

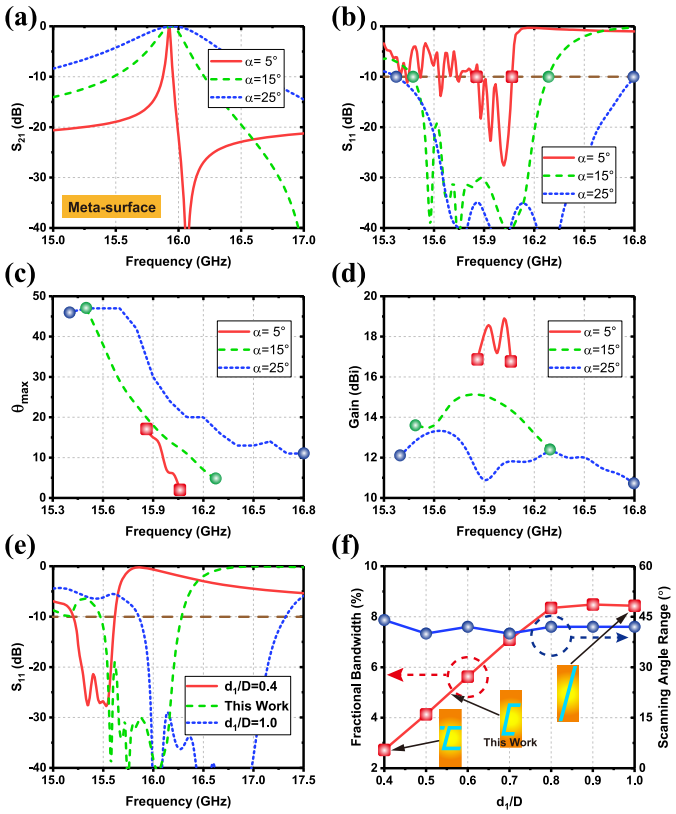

Fig. 5. Matching and bandwidth properties of the TWSAA. (a) Transmission coefficients of the metasurface at the incident angle of $\theta = 15°$ with different oblique angles α of the C-slits. (b) Reflection coefficients of the TWSAA with different oblique angles α of the C-slits. (c) and (d) Main lobe directions and gains of the TWSAA in the operating frequency range with different oblique angles α of the C-slits. (e) Reflection coefficients of the TWSAA with different d_1/D when $D = 8.1$ mm. (f) Operating FBW and scanning angle range varied with d_1/D when $D = 8.1$ mm. In (a), other metasurface parameters are the same as shown in Fig. 1(c). In (b)–(f), other antenna parameters are the same as shown in Fig. 3.

where F_n is the transmission amplitude of the nth C-slit to emit EM fields with the radiating direction determined as

$$\beta p - kp \sin\theta_f = \pm 2m\pi (m = 0, 1, 2 \cdots). \tag{7}$$

In the case of very small separation p between the adjacent C-slits, the value of m would be 0 and the radiating direction would be

$$\theta_f = \arccos\left(\frac{\lambda_0}{2W_x}\right). \tag{8}$$

From (4) and (8), we can observe that the incident angle θ_x in the waveguide and the radiating direction θ_f from the TWSAA are consistent when p is very small. Therefore, the scanning range would theoretically have

$$0 \le \theta_f \le \arccos\left(\frac{\lambda_0}{2W_1}\right) \tag{9}$$

where the maximum value of θ_f would reach 51°, 54°, and 56° when the TWSAA is operating at 15, 16, and 17 GHz, respectively.

Fig. 4 demonstrates the near-field distributions and 3-D far-field radiation patterns of the TWSAA at different frequencies. We can observe that the TE_{10} mode could penetrate the metasurface at different positions and radiate the EM waves in different directions as the frequency changes. The main lobe is steering at 47°, 23°, and 7°, respectively, when the antenna is working at 15.5, 15.8, and 16.2 GHz, demonstrating the perfect frequency scanning performance. The maximum gains of the proposed design are 13.6, 15.1, and 13.2 dBi with the 3 dB beamwidths of 9.1°, 8.1°, and 14.4°, respectively, at 15.5, 15.8, and 16.2 GHz. The antenna gains are not high compared with the traditional rectangular waveguide slot array antenna having the same aperture. This is because not all of the C-slits are utilized to radiate EM fields at a given frequency, and we can see it clearly in Fig. 4 that only parts of the SAF metasurface participates in the radiation for a specific frequency due to the equivalent incident angles are different at different positions of the tapered waveguide. However, the whole aperture of the SAF metasurface would contribute to the entire radiations when the radiating beam starts to steer within the given frequency range for the frequency-scanning design.

In order to use a specific frequency band to perform the scanning radiation, a good impedance matching of the TWSAA should first be guaranteed. Fig. 5(a) demonstrates that the transmission bandwidth of the SAF metasurface would become narrower as the oblique angles α of the C-slits decreases. Similarly, the reflection coefficients of the TWSAA would increase and the impedance matching would be seriously deteriorated when α reduces to 5° from 25°, as can be observed in Fig. 5(b) and (c), and the scanning range would also shrink greatly as the operating frequency range from 15.86 to 16.06 GHz is clearly limited. With the aim to have a better impedance matching performance, we can

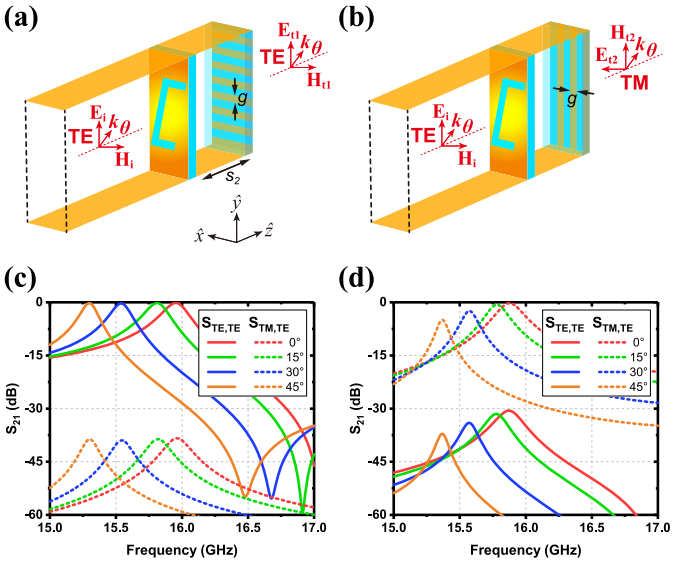

Fig. 6. SAF metasurfaces with the polarization selective surfaces and their transmission characteristics. (a) First unit cell of the metasurface for TE_y transmitted EM waves. (b) Second unit cell of the metasurface for TM_y transmitted EM waves. The transmission coefficients for the (c) First and (d) Second unit cell with the oblique incidence of TE_y-polarized EM fields, where the structural parameters are $g = 0.5$ mm, $s_2 = 7$ mm, and other parameters are the same as in shown Fig. 1(c).

increase α to enable the C-slits to radiate the EM fields easily. However, such a strategy would lead to fewer C-slits participating the radiations with the decrease of the antenna gains, as shown in Fig. 5(d). Therefore, a proper value of α is required to balance the impedance matching and radiation performances, such as $\alpha = 15°$ in our design. In addition, given a specific scanning range of the antenna radiations, the coupling intensity between the symmetrical oblique C-slits would function as the key issue to control the operating frequency band. We can observe in Fig. 5(e) that the operating bandwidth of the TWSAA would be 0.42 and 1.40 GHz when $d_1/D = 0.4$ and $d_1/D = 1$, respectively. Through adjusting the ratio d_1/D of the C-slits, the operating FBW could be tuned from 2.7% to 8.5% when d_1/D increases from 0.4 to 1, as shown in Fig. 5(f), where the scanning angle range keeps almost unchanged around 40°.

The present design now can obtain the frequency scanning performance in a narrow frequency band with the TE_y polarized radiations. However, it is required to use the long transitional parallel PEC boundaries to mimic the symmetrical C-slits, otherwise the TWSAA would not produce the frequency scanning performance. To solve this problem, we can add metal gratings behind the SAF metasurface [26], which could effectively reduce the length s_2 of the transitional parallel PEC boundaries, as shown in Fig. 6(a) and (b). In addition, the metasurfaces with different directional metal gratings can also transmit two orthogonally TE_y-polarized and TM_y-polarized EM fields under the same illuminations of the TE_y-polarized EM fields, where the metal gratings are printed on the dielectric substrate ($\varepsilon_r = 2.65$) to form the polarization selective surfaces. We can observe in Fig. 6(c) that the frequency of the transmitted TE_y-polarized EM fields

TABLE I
COMPARISONS BETWEEN TRADITIONAL WAVEGUIDE SLOT ARRAY ANTENNAS AND TWSAAS

Antennas	Frequency (GHz)	FBW	Scanning angle range (°)
Tradi.	15.5-16.3	5.0%	3.4
TWSAA			42.0
Tradi.	15.5-16.1	3.8%	2.6
$TWSAA_1^{TE}$			34.0
Tradi.	15.5-16.0	3.2%	2.2
$TWSAA_2^{TM}$			36.0

for the first unit cell can be tuned from 15.95 to 15.30 GHz when the incident angle is swept from 0° to 45° with very small transmitted TM_y-polarized EM fields. The transmitted TE_y-polarized EM waves can be expressed as

$$\begin{cases} \vec{E}_{t1} = E_{t1}\hat{y}e^{-jk(x\sin\theta+z\cos\theta)} \\ \vec{H}_{t1} = \dfrac{E_{t1}}{\eta}(-\hat{x}\cos\theta+\hat{z}\sin\theta)e^{-jk(x\sin\theta+z\cos\theta)}. \end{cases} \tag{10}$$

In addition, we can also observe in Fig. 6(d) that the frequency of the transmitted TM_y-polarized EM fields for the second unit cell can be tuned from 15.88 to 15.37 GHz when the incident angle is swept from 0° to 45°, achieving the conversion of the TE_y to the TM_y-polarized EM fields and also with very small transmitted TE_y-polarized EM fields. The transmitted TM_y-polarized EM waves can be expressed as

$$\begin{cases} \vec{E}_{t2} = E_{t2}(\hat{x}\cos\theta-\hat{z}\sin\theta)e^{-jk(x\sin\theta+z\cos\theta)} \\ \vec{H}_{t2} = \dfrac{E_{t2}}{\eta}\hat{y}e^{-jk(x\sin\theta+z\cos\theta)}. \end{cases} \tag{11}$$

We continue to apply the SAF metasurface with such polarization selective surfaces to the narrow side of the tapered waveguide to form two TWSAAs, as shown in Fig. 7(a) and (b), to have the radiation of two orthogonally TE_y-polarized and TM_y-polarized EM fields and simultaneously with the frequency scanning performances. We can observe in Fig. 7(c) and (d) that the reflection coefficients are less than -10 dB with good impedance matching in the frequency range approximately from 15.5 to 16.1 GHz for the $TWSAA_1^{TE}$ and from 15.5 to 16.0 GHz for the $TWSAA_2^{TM}$. In the meanwhile, as shown in Fig. 7(e) and (f), we can observe that the main lobes can scan from 39° to 5° with 3.8% FBW for the $TWSAA_1^{TE}$ and from 41° to 5° with 3.2% FBW for the $TWSAA_2^{TM}$, where both TWSAAs have realized the frequency scanning of the radiation beams in a narrow frequency band. Therefore, our design would achieve the reduced size and convert the polarization of radiation beams simultaneously when supplemented with the polarization selective surfaces.

Table I demonstrates the comparisons between the traditional waveguide slot array antennas and TWSAAs. We can observe that the scanning angle range of TWSAAs is much greater than traditional waveguide slot array antennas within the same bandwidths. Such a characteristic of wide angular scanning within a narrow frequency band should be very useful, especially for the increasing limited frequency spectrum in wireless communications.

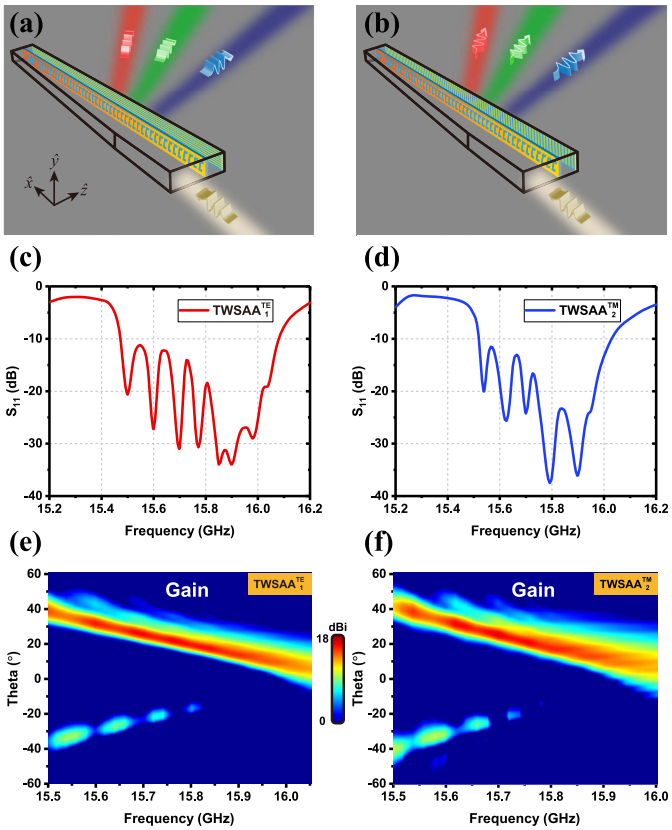

Fig. 7. Illustration of the TWSAAs using the SAF metasurfaces with the polarization selective surfaces. (a) Demonstration of the TWSAA$_1^{TE}$ for TE$_y$ radiated waves. (b) Demonstration of the TWSAA$_2^{TM}$ for TM$_y$ radiated waves. (c) and (d) Reflection coefficients of the TWSAAs. (e) and (f) Far-field radiation performances of the TWSAAs in xz-plane. In (c)–(f), Waveguide parameters are the same as shown in Fig. 3, and the metasurface parameters are the same as shown in Fig. 6.

V. Fabrication and Experimental Tests

Finally, we fabricate the proposed TWSAAs and experimentally test their radiation performances, as demonstrated in Figs 8–10. In the fabrication, the TWSAA is synthesized through three tightly connected metal plates and an SAF metasurface. We use a 0.5 mm groove on the top metal plate and another identical groove on the bottom metal plate to fix the SAF metasurface, and the F4B circuit board (ε_r = 2.65 and loss tangent = 0.001) is chosen as the dielectric substrate for the metasurface. The supporting metal plate sandwiched in the top and bottom parallel plates is fabricated in a tapered shape so as to make s_1 varied and s_2 unchanged for the excitation of the oblique incident waves in the tapered rectangular waveguide, as shown in Fig. 8. The TWSAA$_1^{TE}$ and TWSAA$_2^{TM}$ are fabricated following the similar process of the TWSAA but the difference is that TWSAA$_1^{TE}$/TWSAA$_2^{TM}$ would have four grooves in total to fix both the SAF metasurface and the polarization selective surface with largely reduced length of s_2. The operating frequencies of the TWSAAs in Fig. 9 are approximately from 15.9 to 16.8 GHz. Within such a frequency range, TWSAA scans in the directions of 16°, 36°, and 51° at 16.8, 16.4, and 16.0 GHz, respectively, achieving a 35° scanning angle range with 4.9% FBW.

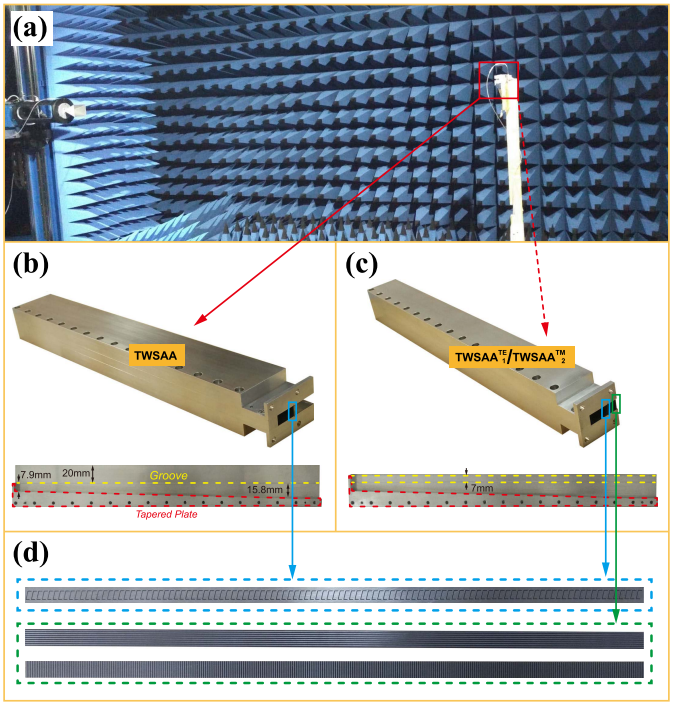

Fig. 8. Experimental setup and manufactured photographs of the TWSAAs. (a) Experimental setup. (b) and (c) Manufactured photos of the TWSAAs. (d) Manufactured photographs of the metasurface and polarization selective surfaces.

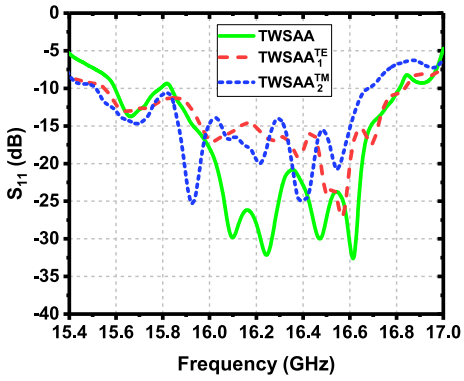

Fig. 9. Measured reflection coefficients of the TWSAAs.

In addition, TWSAA$_1^{TE}$ scans in the directions of 8°, 28°, and 45° at 16.7, 16.4, and 16.1 GHz, respectively, achieving a 37° scanning angle range with 3.7% FBW, while the radiations of the TM-polarized patterns are very small with less than −10 dBi gains. Similarly, TWSAA$_2^{TM}$ scans in the directions of 7°, 30°, and 46° at 16.5, 16.2, and 16.0 GHz, respectively, achieving a 39° scanning angle range with 3.1% FBW, while the radiations of the TE-polarized patterns are very small with less than −5 dBi gains. We can observe that the operating frequencies of the measured results are shifted about 0.5 GHz compared with the simulated results, which mainly come from the fabrication errors of the metal plates and the metasurface. Besides, the sidelobe levels of measured results are a little higher than the simulated results, which are mainly caused by the leakages from the gaps between the metal plates in the fabrication of the rectangular waveguide,

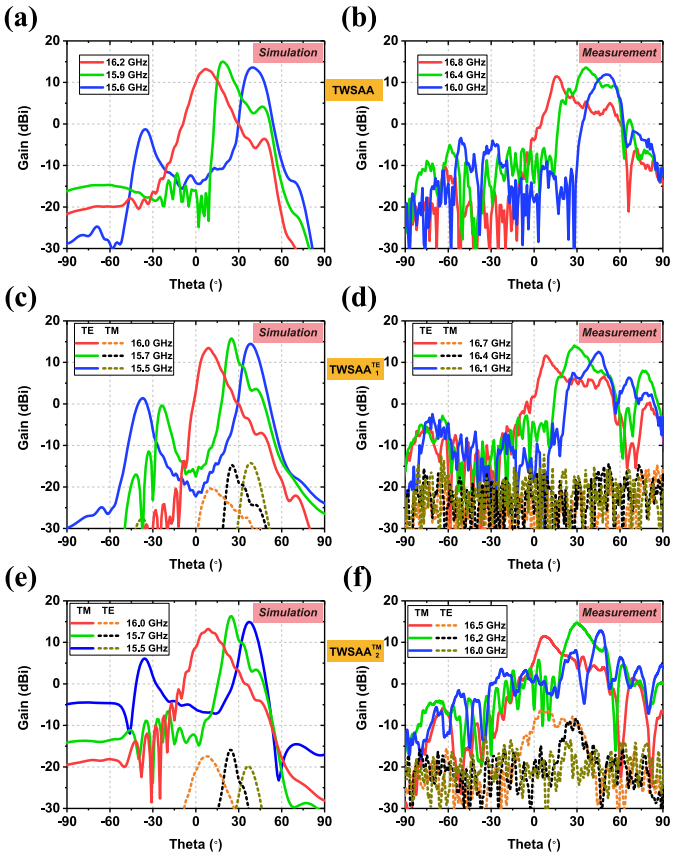

Fig. 10. Simulated and measured far-field patterns of the TWSAAs in *xz*-plane. (a) and (b) TWSAA. (c) and (d) TWSAA$_1^{TE}$. (e) and (f) TWSAA$_2^{TM}$.

whereas, we assume they are perfectly connected in the simulations. Nevertheless, the measured results still show the excellent frequency scanning and polarization conversion performances of the TWSAAs, which further verifies our proposed designs.

VI. Conclusion

In conclusion, we have proposed three SAF metasurface-based TWSAAs for the frequency scanning in this paper. The metasurface composed of oblique C-slits is shown to be capable of releasing different wavelength energies when under the illumination of TE-polarized plane waves from different incident angles, while the tapered waveguide is proposed to mimic the oblique incidence and thus functions as the excitation of the antenna. Such frequency scanning radiations can also be extended for both orthogonally polarized EM fields when integrated with another polarization selective surface properly behind the metasurface. Our designs of SAF metasurface-based TWSAAs should provide a new route to design novel frequency scanning antennas and also waveguide slot array antennas.

References

[1] G. Gentile *et al.*, "Silicon-filled rectangular waveguides and frequency scanning antennas for mm-wave integrated systems," *IEEE Trans. Antennas Propag.*, vol. 61, no. 12, pp. 5893–5901, Dec. 2013.

[2] E. D. Cullens, L. Ranzani, K. J. Vanhille, E. N. Grossman, N. Ehsan, and Z. Popovic, "Micro-fabricated 130–180 GHz frequency scanning waveguide arrays," *IEEE Trans. Antennas Propag.*, vol. 60, no. 8, pp. 3647–3653, Aug. 2012.

[3] M. Navarro-Tapia, J. Esteban, and C. Camacho-Penalosa, "On the actual possibilities of applying the composite right/left-handed waveguide technology to slot array antennas," *IEEE Trans. Antennas Propag.*, vol. 60, no. 5, pp. 2183–2193, May 2012.

[4] M. Al Sharkawy and A. A. Kishk, "Wideband beam-scanning circularly polarized inclined slots using ridge gap waveguide," *IEEE Antennas Wireless Propag. Lett.*, vol. 13, pp. 1187–1190, 2014.

[5] N. K. Host, C.-C. Chen, J. L. Volakis, and F. A. Miranda, "Ku-band traveling wave slot array scanned via positioning a dielectric plunger," *IEEE Trans. Antennas Propag.*, vol. 63, no. 12, pp. 5475–5483, Dec. 2015.

[6] P. Sánchez-Olivares and J. L. Masa-Campos, "Novel four cross slot radiator with tuning vias for circularly polarized SIW linear array," *IEEE Trans. Antennas Propag.*, vol. 62, no. 4, pp. 2271–2275, Apr. 2014.

[7] W. Cao, Z. N. Chen, W. Hong, B. Zhang, and A. Liu, "A beam scanning leaky-wave slot antenna with enhanced scanning angle range and flat gain characteristic using composite phase-shifting transmission line," *IEEE Trans. Antennas Propag.*, vol. 62, no. 11, pp. 5871–5875, Nov. 2014.

[8] Y. J. Cheng, W. Hong, and K. Wu, "Millimeter-wave half mode substrate integrated waveguide frequency scanning antenna with quadri-polarization," *IEEE Trans. Antennas Propag.*, vol. 58, no. 6, pp. 1848–1855, Jun. 2010.

[9] O. Bayraktar and O. A. Civi, "Circumferential traveling wave slot array on cylindrical substrate integrated waveguide (CSIW)," *IEEE Trans. Antennas Propag.*, vol. 62, no. 7, pp. 3557–3566, Jul. 2014.

[10] X.-X. Yang, L. Di, Y. Yu, and S. Gao, "Low-profile frequency-scanned antenna based on substrate integrated waveguide," *IEEE Trans. Antennas Propag.*, vol. 65, no. 4, pp. 2051–2056, Apr. 2017.

[11] R. J. Mailloux, *Phased Array Antenna Handbook*, 2nd ed. Norwood, MA, USA: Artech House, 2005.

[12] N. Yu *et al.*, "Light propagation with phase discontinuities: Generalized laws of reflection and refraction," *Science*, vol. 334, no. 6054, pp. 333–337, Oct. 2011.

[13] Y. B. Li, X. Wan, B. G. Cai, Q. Cheng, and T. J. Cui, "Frequency-controls of electromagnetic multi-beam scanning by metasurfaces," *Sci. Rep.*, vol. 4, Nov. 2014, Art. no. 6921.

[14] S.-W. Qu *et al.*, "Controlling dispersion characteristics of terahertz metasurface," *Sci. Rep.*, vol. 5, Mar. 2015, Art. no. 9367.

[15] S. Pandi, C. A. Balanis, and C. R. Birtcher, "Analysis of wideband multi-layered sinusoidally modulated metasurface," *IEEE Antennas Wireless Propag. Lett.*, vol. 15, pp. 1491–1494, 2016.

[16] B. Cheng, D. Liu, J. Wu, and H. Li, "Frequency scanning non-diffraction beam by metasurface," *Appl. Phys. Lett.*, vol. 110, p. 031108, Jan. 2017.

[17] T. J. Cui, M. Q. Qi, X. Wan, J. Zhao, and Q. Cheng, "Coding metamaterials, digital metamaterials and programmable metamaterials," *Light-Sci. Appl.*, vol. 3, p. e218, Oct. 2014.

[18] X. Wan, M. Q. Qi, T. Y. Chen, and T. J. Cui, "Field-programmable beam reconfiguring based on digitally-controlled coding metasurface," *Sci. Rep.*, vol. 6, Feb. 2016, Art. no. 20663.

[19] L. Li *et al.*, "Electromagnetic reprogrammable coding-metasurface holograms," *Nature Commun.*, vol. 8, Aug. 2017, Art. no. 197.

[20] S. Liu and T. J. Cui, "Flexible controls of terahertz waves using coding and programmable metasurfaces," *IEEE J. Sel. Topics Quantum Electron.*, vol. 23, no. 4, Jul./Aug. 2017, Art. no. 4700312.

[21] B. A. Munk, *Frequency Selective Surfaces: Theory and Design*. Hoboken, NJ, USA: Wiley, 2005.

[22] P. B. C. Medeiros, V. P. S. Neto, and A. G. D'Assunção, "A compact and stable design of FSS with radial slit circular elements using an iterative method," *Microw. Opt. Technol. Lett.*, vol. 57, no. 3, pp. 729–733, Mar. 2015.

[23] J. D. Ortiz, J. D. Baena, V. Losada, F. Medina, and J. L. Araque, "Spatial angular filtering by FSSs made of chains of interconnected SRRs and CSRRs," *IEEE Microw. Wireless Compon. Lett.*, vol. 23, no. 9, pp. 477–479, Sep. 2013.

[24] J. D. Ortiz, J. P. del Risco, J. D. Baena, V. Losada, F. Medina, and J. L. Araque, "Metasurfaces for angular filtering and beam scanning," in *Proc. 8th Int. Congr. Adv. Electromagn. Mater. Microw. Opt. (METAMATERIALS)*, Aug. 2014, pp. 34–36.

[25] J.-S. Hong and M. J. Lancaster, "Couplings of microstrip square open-loop resonators for cross-coupled planar microwave filters," *IEEE Trans. Microw. Theory Techn.*, vol. 44, no. 11, pp. 2099–2109, Nov. 1996.
[26] N. K. Grady *et al.*, "Terahertz metamaterials for linear polarization conversion and anomalous refraction," *Science*, vol. 340, no. 6138, pp. 1304–1307, 2013.

Aofang Zhang was born in Bozhou, Anhui, China, in 1993. He received the B.Eng. degree in electromagnetic wave propagation and antenna from the School of Physics and Optoelectronic Engineering, Xidian University, Xi'an, China, in 2014, where he is currently pursuing the Ph.D. degree in electromagnetic field and microwave technology with the School of Electronic Engineering.

His current research interests include metamaterials, metasurfaces, phased array antennas, frequency scanning antennas, waveguide slot array antennas, and circularly polarized array antennas.

Rui Yang received the Ph.D. degree in electromagnetic fields and microwave technology from Xidian University, Xi'an, China, in 2008.

He joined the School of Electronic Engineering, Xidian University, in 2008, and was promoted to an Associate Professor in 2012 and a Professor in 2017. From 2009 to 2011, he visited Queen Mary, University of London, London, U.K., as a Newton Research Fellow. His current research interests include the electromagnetic metamaterials and their applications in the microwave circuits and antennas.

Dr. Yang was a recipient of the Newton International Fellowship.

Dong Li was born in Xi'an, Shaanxi, China, in 1992. He received the B.Eng. degree in electronic and information engineering from the School of Electronic Engineering, Xidian University, Xi'an, in 2015, where he is currently pursuing the M.Eng. degree in electromagnetic field and microwave technology.

His current research interests include metasurfaces, vortex electromagnetic fields, reflectarray antennas, and band-notch antennas.

Bowei Hu was born in Xianyang, Shaanxi, China, in 1992. He received the B.Eng. degree in electronic and information engineering from the North University of China, Taiyuan, China, in 2014. He is currently pursuing the M. Eng. degree in electronics and communications engineering from the School of Electronic Engineering, Xidian University, Xi'an, China.

His current research interests include metamaterials, subwavelength imaging, and waveguide filters.

Zhenya Lei received the B.Eng. and M.Eng. degrees in electrical engineering from Xidian University, Xi'an, China, in 1981 and 1999, respectively.

Since 1981, he has been involved in teaching and research of electromagnetic field and microwave technology with Xidian University, where he is currently a Professor and the Head of the Microwave Research Institute. His current research interests include micorwave circuits, antenna design and fabrication engineering, computational electromagnetics, and metamaterials.

Mr. Lei is the Director of Microwave and Radio Wave Propagation Committee of the Shaanxi Institute of Electronics. He was also the Deputy Director of the Microwave Teaching and Research Office.

Yongchang Jiao received the B.S. degree in mathematics from Shanxi University, Taiyuan, China, in 1984, and the M.S. degree in applied mathematics and the Ph.D. degree in electrical engineering from Xidian University, Xi'an, China, in 1987 and 1990, respectively.

In 1990, he joined the Institute of Antennas and EM scattering, Xidian University, where he is currently a Professor. In 1996, he was supported by the Japan Society or the Promotion of Science and worked as a Visiting Priority-Area Research Fellow with the University of Tsukuba, Tsukuba, Japan. From 1997 to 1998 and from 1999 to 2000, he was a Research Associate with the Chinese University of Hong Kong, Hong Kong. In 2002, he was a Research Fellow with the City University of Hong Kong, Hong Kong. His current research interests include antenna array, antenna design, computational electromagnetics, optimization algorithms and applications, and evolutionary computation.